Am J Physiol Renal Physiol 296: F751–F761, 2009.
First published December 30, 2008; doi:10.1152/ajprenal.90669.2008.

Electrotonic vascular signal conduction and nephron synchronization

Donald J. Marsh,[1] Ildiko Toma,[2] Olga V. Sosnovtseva,[3] Janos Peti-Peterdi,[2] and Niels-Henrik Holstein-Rathlou[4]

[1]*Department of Molecular Pharmacology, Physiology, and Biotechnology, Brown University, Providence, Rhode Island;* [2]*Department of Physiology and Biophysics, Zilkha Neurogenetic Institute, University of Southern California, Los Angeles, California;* [3]*Department of Physics, Danish Technical University, Lyngby; and* [4]*Department of Biomedical Sciences, University of Copenhagen, Copenhagen, Denmark*

Submitted 11 November 2008; accepted in final form 23 December 2008

Marsh DJ, Toma I, Sosnovtseva OV, Peti-Peterdi J, Holstein-Rathlou NH. Electrotonic vascular signal conduction and nephron synchronization. *Am J Physiol Renal Physiol* 296: F751–F761, 2009. First published December 30, 2008; doi:10.1152/ajprenal.90669.2008.—Tubuloglomerular feedback (TGF) and the myogenic mechanism control afferent arteriolar diameter in each nephron and regulate blood flow. Both mechanisms generate self-sustained oscillations, the oscillations interact, TGF modulates the frequency and amplitude of the myogenic oscillation, and the oscillations synchronize; a 5:1 frequency ratio is the most frequent. TGF oscillations synchronize in nephron pairs supplied from a common cortical radial artery, as do myogenic oscillations. We propose that electrotonic vascular signal propagation from one juxtaglomerular apparatus interacts with similar signals from other nephrons to produce synchronization. We tested this idea in tubular-vascular preparations from mice. Vascular smooth muscle cells were loaded with a fluorescent voltage-sensitive dye; fluorescence intensity was measured with confocal microscopy. Perfusion of the thick ascending limb activated TGF and depolarized afferent arteriolar smooth muscle cells. The depolarization spread to the cortical radial artery and other afferent arterioles and declined with distance from the perfused juxtaglomerular apparatus, consistent with electrotonic vascular signal propagation. With a mathematical model of two coupled nephrons, we estimated the conductance of nephron coupling by fitting simulated vessel diameters to experimental data. With this value, we simulated nephron pairs to test for synchronization. In single-nephron simulations, the frequency of the TGF oscillation varied with nephron length. Coupling nephrons of different lengths forced TGF frequencies of both pair members to converge to a common value. The myogenic oscillations also synchronized, and the synchronization between the TGF and the myogenic oscillations showed an increased stability against parameter perturbations. Electronic vascular signal propagation is a plausible mechanism for nephron synchronization. Coupling increased the stability of the various oscillations.

renal autoregulation; tubuloglomerular feedback; myogenic mechanism; coupled oscillators; coupled nephrons; stability

THE MYOGENIC MECHANISM AND tubuloglomerular feedback (TGF) act together to provide autoregulation of renal blood and glomerular filtration rate (GFR). Each mechanism oscillates in normal animals; the TGF oscillation has the larger amplitude and longer period length of the two (13). The oscillations are the result of nonlinearities in each system, and these two mechanisms interact because they act on a single contractile mechanism in arteriolar smooth cells (21). The interactions lead to synchronization of the oscillations and modulation of the frequency and amplitude of the myogenic mechanism by TGF (23). Because of the synchronization between the myogenic and the TGF oscillations, the frequencies of the two oscillations operate with a fixed ratio in the individual nephron, a 5:1 ratio being the most frequent.

The TGF and myogenic oscillations in adjacent nephrons also synchronize (33, 37). Adjacent in this context means that the nephrons are supplied with blood from a common cortical radial artery. TGF activation in a single nephron is known to cause a similar but smaller response in adjacent nephrons (4, 15, 26). Synchronization is a well-known phenomenon (27) found in many nonlinear oscillating physical and biological systems. The concept has been especially fruitful when applied to studies of brain function (30–32), but the study of the phenomenon in the kidney is just beginning. Synchronization facilitates the aggregation of small units, such as nephrons, into larger ones, and new properties often emerge from the ensemble.

In this study, we tested two hypotheses about the mechanism of nephron-nephron synchronization: that activation of TGF induces depolarization of vascular smooth muscle cells which propagates away from the juxtaglomerular apparatus and that the depolarization is a plausible mechanism for synchronization. We used a voltage-sensitive fluorescent dye in the perfused mouse juxtaglomerular apparatus and found that TGF activation initiates a change in membrane potential of smooth muscle cells in afferent arterioles. The depolarization propagates away from the juxtaglomerular apparatus and into adjacent afferent arterioles. We then used a mathematical model of TGF-myogenic interactions (21) to determine the magnitude of the electrical resistance between adjacent nephrons by fitting a two-nephron model to experimental data (35), and we used the result to test for synchronization. The two-nephron model shows synchronization of both TGF and myogenic oscillations between nephrons of different lengths. Without coupling, the frequency of the TGF oscillation depends on tubule length, and the frequencies of the myogenic oscillations are also different in the two nephrons because of the synchronization between myogenic and TGF oscillations in each nephron (33). With coupling, the TGF frequency of both nephrons shifts to a common value, and the synchronization of TGF with the myogenic oscillation remains at 5:1. These results support the suggestion that vascular electrical conduction permits the synchronization phenomena that have been observed in experiments. In addition, the model permits us to predict the stability of synchronization, which is enhanced by nephron-to-nephron coupling.

Address for reprint requests and other correspondence: D. J. Marsh, Dept. of Molecular Pharmacology, Physiology, and Biotechnology, Brown University, Box G-B3, Providence, RI 02912 (e-mail: marsh@ash.biomed.brown.edu).

The costs of publication of this article were defrayed in part by the payment of page charges. The article must therefore be hereby marked "*advertisement*" in accordance with 18 U.S.C. Section 1734 solely to indicate this fact.

MATERIALS AND METHODS

Animal experiments: in vitro isolated, perfused juxtaglomerular apparatus. Afferent arterioles with attached glomerulus and distal tubule containing the macula densa (JGA complex) were dissected from among the most superficial nephrons in the cortex of C57/BL6 mice [6 wk of age, from our colony at the University of Southern California (USC)] and microperfused as described in a previous report (26). All animal protocols were conducted in accordance with the guidelines published by the American Physiological Society and were approved by the Institutional Animal Care and Use Committee of USC, where all the experiments were conducted. The dissection medium was prepared from a DMEM/F-12 mixture (Sigma). Fetal bovine serum (Hyclone) was added at a final concentration of 3%. Each preparation was transferred to a thermoregulated Lucite chamber mounted on a Leica IRE2 inverted microscope. Bath fluid was a modified Krebs-Ringer-HCO_3 buffer containing (in mM) 115 NaCl, 25 $NaHCO_3$, 0.96 NaH_2PO_4, 0.24 Na_2HPO_4, 5 KCl, 1.2 $MgSO_4$, 2 $CaCl_2$, 5.5 D-glucose and 100 μM L-arginine. The tubular perfusate was an isosmotic, low NaCl containing Ringer's solution consisting of (in mM) 10 NaCl, 135 *N*-methyl-D-glucamine (NMDG) cyclamate, 5 KCl, 1 $MgSO_4$, 1.6 Na_2HPO_4, 0.4 NaH_2PO_4, 1.5 $CaCl_2$, 5 D-glucose, and 10 HEPES. The tubule segment containing the macula densa was cannulated separately and perfused at a baseline rate of ~2 nl/min. The solutions were aerated with 95% O_2-5% CO_2 for 45 min, and their pH was adjusted to 7.4. The bath was exchanged at a rate of 1 ml/min. The preparation was kept in the dissection solution at an initial temperature of 4°C until cannulation of the tubule was completed, at which point the temperature was raised gradually to 37°C and maintained at that level for the remainder of the experiment. TGF was activated by raising the NaCl concentration in the tubule perfusate from 10 to 80 mM for a period of 10–15 s (26). Isosmolality was maintained by reducing NMDG cyclamate.

Multiphoton fluorescence microscopy. Preparations were visualized using a two-photon excitation laser-scanning confocal fluorescence microscope (TCS SP2 AOBS MP confocal microscope system, Leica-Microsystems, Heidelberg, Germany). A Leica DM IRE2 inverted microscope was powered by a wideband, fully automated, infrared (710–920 nm) combined photo-diode pump laser and mode-locked titanium:sapphire laser (Mai-Tai, Spectra-Physics) for multiphoton excitation. Images were collected in time series at 2.5 Hz and analyzed with the Leica LCS imaging software (LCS 2.61.1537) Quantification Tools. Vascular smooth muscle cells of the afferent arteriole were loaded from the bath with ANNINE-6, a newly synthesized voltage-sensitive dye designed for ultrafast (1 ms) neural signal detection (17). ANNINE-6 was dissolved in 20% Pluronic F-127 DMSO (Sigma) at a concentration of 0.5 mg/ml (dye stock solution), which was added to the bath solution diluted 1:100 for 10 min and then washed out. ANNINE-6 is highly membrane specific and responds to a membrane-depolarizing voltage with a fluorescence decrease (17). ANNINE-6 was excited at 920 nm using the two-photon laser, and fluorescence was detected in the range of 520–800 nm.

Simulations. Simulations were conducted with the model presented previously (21) and which is in the APPENDIX. Tables of the parameter values used to solve the model are given in Supplemental Materials (the online version of the article contains supplemental data). Three changes were made to the equation structure of the previous model: the addition of the coupling current to the differential equations simulating membrane currents (*Eqs. A21* and *A22*); the addition of a nephron-coupling network; and the use of nephrons of variable length. New parameters were the conductance coupling the two nephrons through an electrical node and a conductance of the node to ground. The model was otherwise used unmodified from its original form, with respect to both equation structure and all parameter values but one. The exception is φ_n, which sets the time course of the fraction of open K-channel states (*Eq. A20*) and is used to modify the frequency of myogenic oscillations to permit synchronization with the TGF oscillation. Some of the numerical methods have been improved, as detailed below.

In brief, the model solves three partial differential equations which express the change in tubular pressure, flow, and NaCl concentration with respect to time and length along the nephron (*Eqs. A1*, *A2*, and *A7*). The tubular wall is mechanically compliant (*Eq. A6*) and reabsorbs fluid and NaCl (*Eqs. A4*, *A5*, and *A8*). The NaCl concentration at the region of the tubule corresponding to the macula densa is used as a signal to TGF which affects afferent arteriolar diameter (*Eq. A9*). The boundary conditions are glomerular filtration rate, calculated by the model of Deen et al. (9) (*Eqs. A10–A13*); the tubular NaCl concentration at the end of the proximal tubule (fluid reabsorption along the proximal tubule produces no change in Na concentration, and the calculation of NaCl concentration is therefore begun at the beginning of the loop of Henle); and the tubular hydrostatic pressure at the distal end of the tubular model. The tubular resistance in the connecting tubule and the collecting ducts decreases with increasing flow rate because of the tubule's mechanical compliance (20). This relationship, which is critical to the calculation of tubular pressure, is represented in a nonlinear expression (*Eq. A3*).

The time-dependent behavior of the smooth muscle cells of the afferent arterioles is simulated by a system of six ordinary differential equations that express the rate of change with respect to time of the fraction of open membrane K^+ channels (*Eqs. A17–A20*), the intracellular Ca^{2+} concentration (*Eqs. A16*, *A24–A26*), the membrane electrical potential difference (PD; *Eqs. A21* and *A22*), the fraction of actin-myosin cross bridges (*Eq. A28*), the mechanical force of contraction (*Eqs. A29–A32*), and the arteriolar diameter (*Eqs. A33–A37*), all as functions of time. The K^+ channels are Ca^{2+} and voltage sensitive (*Eqs. A17* and *A18*), and the Ca^{2+} channels are voltage sensitive (*Eq. A24*). Intracellular Ca^{2+} governs the phosphorylation of myosin light chain (*Eq. A27*), and the fraction of actin-myosin cross bridges is a function of the fraction of phosphorylated sites on myosin light chain (*Eq. A28*). The force of contraction is dependent on the number of cross bridges and the length of the contractile mechanism (*Eq. A32*), and the circumferential length of the smooth muscle cells is a resultant of the stresses from the contractile and elastic elements of the cells, and the action of the local pressure difference across the arteriolar wall. The behavior of these variables along the length of the afferent arteriole is approximated by making the calculations in two segments. The segment closer to the glomerulus receives the larger fraction of the TGF input. In the model, this segment accounts for one-third of the total length of the afferent arteriole. The two segments are electrically coupled. TGF input is used to modulate the membrane Ca^{2+} conductance. The vascular resistance of the afferent arteriole is calculated from the diameters of the two segments, under the assumption that the resistance varies inversely with the fourth power of the diameter. The complete model simulates both TGF and myogenic oscillations at measured frequencies and amplitudes; it also predicts their synchronization at a frequency ratio of 5:1 and modulation of the amplitude and frequency of the myogenic oscillation by TGF. These phenomena have been observed in experimental data (21, 33).

Electrical coupling between nephrons was simulated with electrical conductances between the proximal ends of the proximal arteriolar segments in each arteriole, connected to a node in the cortical radial artery. The node was connected to ground by a separate conductance which is intended to represent the conductive pathway to other nephrons supplied by the artery and finally to some ground point in the circulation. Current flows at the node were made to sum to zero, in accordance with Kirchhoff's first law.

The original single-nephron model was modified to establish baseline predictions for tubules of different lengths. The single-nephron model used here differed from the version presented (21) only in the numerical methods, as detailed below. The results of this model for cortical nephrons have remained unaltered by the change to the newer methods. The two-nephron model was used to estimate the conduc-

tance of the pathway connecting the two nephrons, and to detect synchronization.

Numerical methods. The partial differential equations describing pressure, flow, and NaCl concentration in each renal tubule were solved using centered difference approximations and are second order correct (34). The spatial step, 2.5×10^{-2} cm (21), was reduced to 1×10^{-2} cm, and the time step was 2.5×10^{-4} s. The auxiliary equations, including the boundary conditions, were solved with the Newton-Raphson method. All calculations were performed in double precision.

The solutions of the ordinary differential equations were obtained with Gear's variable step-size method, using backward differentiation and program-generated Jacobians. This code is from the Livermore National Laboratories, and is available for download at https://computation.llnl.gov/casc/odepack/download/lsode_agree.html. The software has been upgraded and improved from an earlier version, which was used elsewhere (21). Because the solution of the partial differential equations required iterations at each time step, the time steps for the solution of the ordinary differential equations were synchronized with those used for the partial differential equations.

For each time step, the glomerular model was solved by using the afferent resistance and the tubular inlet pressure from the preceding time step as initial estimates. Using the calculated value for GFR for the inflow rate to the tubular system, the pressure, flow, and NaCl equations were solved iteratively within each iteration of the whole system time step. Convergence was assumed when the Euclidian norm of the changes in the combined pressure and flow vectors was $<10^{-3}$ and $<10^{-5}$ for the NaCl concentration vector. The new calculated value for the NaCl concentration at the macula densa was used to estimate the afferent arteriolar resistance. The procedure was repeated, using the new value for the afferent resistance and the tubular inlet pressure, until the system of equations converged. Convergence was assumed when the Euclidean norm of the changes in the afferent resistance was $<10^{-6}$ in successive iterations. Three or four iterations were typically needed to achieve convergence.

Each solution of the model simulated 600–1,200 s. A run that simulated 600 s required ~210 s of machine time on a server with a 3.16-GHz processor and 2 Gb of allocated memory. The runs were sampled at 4 Hz, yielding time series with 4,800 values for 1,200 s.

RESULTS

Perfused juxtaglomerular apparatus. Figure 1 shows microscopic images of dissected afferent arterioles, all branching from a common cortical radial artery. One arteriole supplies a glomerulus, and the perfused segment of tubule containing the macula densa remains attached to the juxtaglomerular apparatus of that glomerulus. The preparation has been bathed in a solution containing the voltage sensitive dye, ANNINE-6. Figure 1*A* contains the control image before TGF stimulation and shows the regions of interest that were sampled; Fig. 1*B* shows the same object as in Fig. 1*A*, but during TGF stimulation. Figure 1*C* is the image acquired from the same object through differential interference contrast optics, and Fig. 1*D* shows the sampled data from each region of interest in Fig. 1*A*.

When the fluid used to perfuse the tubule had its NaCl concentration changed from 10 to 80 mM, each of the three afferent arterioles showed a loss of fluorescence intensity that returned to baseline after the NaCl concentration in the perfusate was returned to 10 mM. The intensity loss was greatest in the arteriole whose macula densa was stimulated and declined with distance from that point, confirming the results of Wagner et al. (35) and Chen et al. (4). Each arteriole also constricted during the period of TGF stimulation. The differential interference contrast images showed that all elements of the preparation remained in focus throughout the sampling period. Although the distance along the arterioles from the first to the third regions of interest was 200 μm, a time lag between them for the depolarization could not be detected. Similar results were obtained in preparations from four mice. The results are consistent with the hypothesis that TGF activation

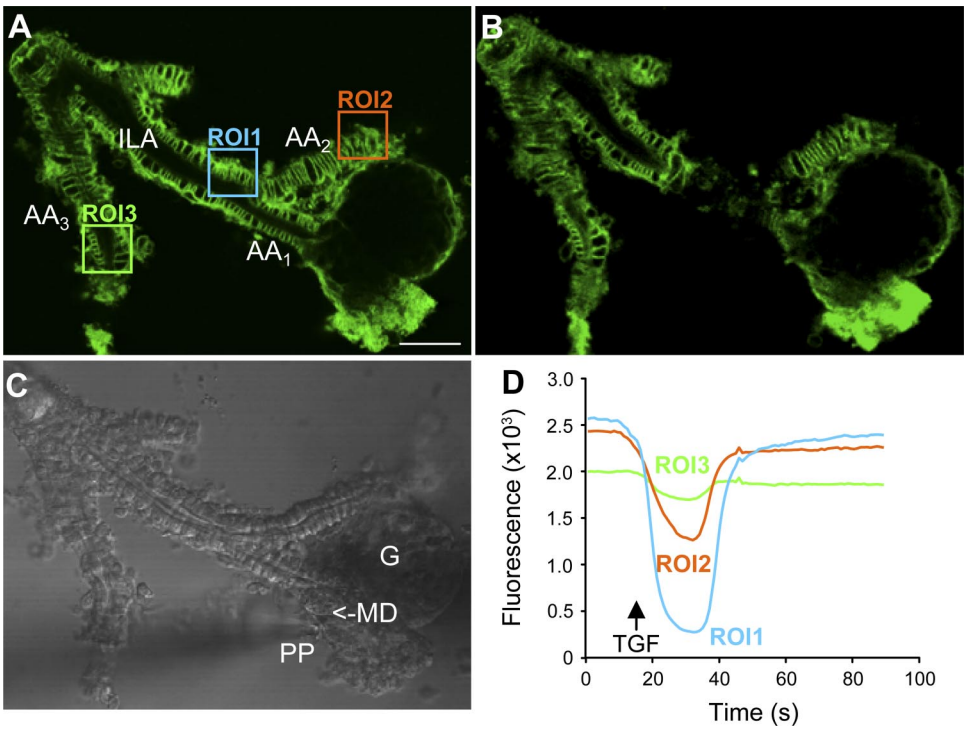

Fig. 1. Direct visualization of propagating tubuloglomerular feedback (TGF)-induced vasoconstrictor and electrical signals in adjacent afferent arterioles (AA) in vitro. ANNINE-6 fluorescence images before (*A*) and after (*B*) TGF stimulation by high NaCl concentration at the macula densa (MD) through a perfusion pipette (PP). *C*: DIC image. G, glomerulus. Fluorescence is highly cell membrane specific and intense in both vascular smooth muscle and endothelial cells. TGF stimulation produced vasoconstriction not only in the parent AA (AA_1) but also in the adjacent arterioles, AA_2 and AA_3. *D*: ANNINE-6 fluorescence measured through the duration of the experiment from each of the regions of interest shown in *A*. Scale bar = 20 μm.

by increased NaCl concentration at the macula densa produces membrane depolarization in vascular smooth muscle cells; that the activation is propagated decrementally along the contiguous vasculature; that each of the visualized segments constricted; and that the depolarization was effectively instantaneous in all segments that could be visualized.

Estimation of nephron-to-nephron coupling strength. Wagner et al. (35) stimulated vasoconstriction in single afferent arterioles in the perfused rat juxtamedullary preparation to measure the magnitude of the propagated response. They stimulated one arteriole near its glomerular end by superfusing a 300 mM KCl-KBr solution over the external surface of the arteriole for 1–5 s and measured vessel diameter at different sites in the stimulated arteriole, in other arterioles, and in the cortical radial artery from which they all derived. The KCl superfusion produced propagated vasoconstriction. The greatest fractional change in diameter occurred at the superfusion site, and the fractional vasoconstriction decreased with distance from the superfusion site. The data set was fitted with the exponential function $y = Ae^{-kx}$, where x is the distance from the stimulation site to the upstream measurement site, y is the diameter change at the distant measurement site, and A is the diameter change at the stimulation site, and k is the inverse of the length constant ($k = 1/\lambda$).

We used the two-nephron model to estimate the conductance needed to achieve the same fractional diameter change as Wagner et al. (35). We simulated the injection of a current pulse of 3 pA for 2 s in the segment of one afferent arteriole closest to the glomerulus. Diameter change was calculated for the arteriolar segments closest to the two glomeruli.

Because the animal experiments were performed using arterioles not showing TGF oscillations, we clamped the value of ϑ, the action of TGF on the afferent arteriole. Typically, ϑ varies over a maximum range -0.4 to 0.4 during a single TGF oscillation when the amplitude of the oscillation is large, which can occur for example at increased blood pressure. At a blood pressure of 100 mmHg, ϑ varies from -0.4 to 0.2. We set ϑ to an arbitrarily selected constant value of -0.25 mmHg·min^{-1}·ml^{-1}, which clamps TGF action at a level equivalent to that produced by a NaCl concentration at the macula densa of 35.7 mM.

The coupling of the nephrons introduces two new parameters, the conductance between the nephrons and the cortical radial artery which is length dependent, and the conductance of the more proximal parts of the renal vasculature to ground. Nordsletten et al. (24) used CT scanning to estimate the lengths, diameters, and numbers of all renal vessels. The average lengths of afferent arterioles they measured was 0.37 mm. The model has two segments of the afferent arteriole connected electrically; the segment closer to the glomerulus is one-third the total length of the arteriole. The segment farther from the glomerulus delivers current to a node connecting the arterioles of the two nephrons. For purposes of the model, therefore, we took the point from which the signal was generated as the border between the two segments in each afferent arteriole so that the distance to the node connecting the two nephrons was 0.245 mm, and the total distance for signal propagation is twice that value, 0.49, under the assumption that the arterioles are identical.

Using the values for the y-intercept, A, and the constant k found by Wagner et al. (35), the ratio y/A at a length of 0.49 mm is 0.24. The ability of the model to achieve this fractional change in diameter of the distal segments of the two nephrons was used as the basis for selecting a value of the internephron coupling conductance.

From the fractional diameter change over a length of 0.49 mm, we calculated the value of the constant k in each simulation and compared it with the experimentally measured value of 2.9 ± 0.5 mm^{-1}. Table 1 compares the effect of changes in the internephron conductance, g_{IN}, with the conductance to ground, g_0, held constant, and Table 2 the effect of changes in g_0 with g_{IN} held constant. The value of g_{IN} that provides the best agreement with the measured value of the constant k is 2.0 pS with g_0 at 2.5×10^{-3} pS, although all values of g_{IN} in Table 2 fall within the range of ± 1 SE of the experimentally measured values. Variation in g_{IN} had a smaller fractional effect on k than did variation in g_0. All further simulations were performed with $g_{IN} = 2.0$ pS and $g_0 = 2.5 \times 10^{-3}$ pS.

Synchronization of nephron oscillations. To detect synchronization it is necessary to show either that the frequencies change from their native values as a result of coupling, or that phase coupling occurs, or both (27). In the simulations to be described, the results are made sufficiently clear with frequency shifts.

To show synchronization, we must start with nephrons that oscillate at different frequencies and that are therefore capable of changing frequency in response to coupling. We modified the model to simulate nephrons of different lengths. The model was originally developed to simulate cortical nephrons of constant length. Medullary nephrons are longer because of the addition of descending and thin ascending limbs of Henle's loop. Table 3 shows the effect of the additional segments on the predicted period lengths and spectral power due to TGF. We have conducted these simulations under the assumption that nephrons of all lengths have both TGF and the myogenic mechanism in place, and that these two oscillations synchronize within each nephron. To achieve this synchronization, we adjusted the value of φ_n , a parameter that adjusts K^+ permeability in *Eq. A20*. Synchronization of TGF and myogenic oscillations has thus far been shown experimentally only in cortical nephrons (33). The ratio of myogenic to TGF frequencies in experimental measurements varies in discrete steps from 4:1 to 6:1; the largest fraction was at 5:1 (33). We started with the value of φ_n that achieves 5:1 synchronization in cortical nephrons and adjusted it to achieve the same synchronization ratio in longer nephrons.

As can be seen in Table 3, nephrons made longer by addition of inner medullary loop of Henle segments have larger and

Table 1. *Effect of variation of g_{IN}, the internephron conductance, on the predicted value of k, the inverse of the length constant, in afferent arterioles*

g_{IN}, pS	k, mm^{-1}
0.5	3.3
1.0	3.1
1.5	3.0
2.0	2.9
2.5	2.8
3.0	2.7
3.5	2.6
4.0	2.6

All simulations were performed with g_0, the conductance to ground, at 2.5×10^{-3} pS and blood pressure set at 100 mmHg.

Table 2. *Effect of variation of g_O, the conductance to ground, on the predicted value of k, the inverse of the length constant, in afferent arterioles*

g_{IN}	k, mm^{-1}
1.5	2.2
2.0	2.6
2.5	2.9
3.0	3.4
3.5	4.1

All simulations were performed with g_{IN} held constant at 2.0 pS and blood pressure set at 100 mmHg.

slower oscillations. The period length increases with tubule length, and so does the amplitude of the TGF oscillation.

Figure 2 shows the predicted renal plasma flow rate as a function of time in two nephrons, one with a descending limb 3 mm long, with the other at 4 mm. In Fig. 2*A*, the nephrons are not coupled. The shorter nephron has a smaller, faster TGF oscillation than the other, and the effect of the myogenic oscillation is seen as five deflections on the TGF oscillation. The longer nephron also shows five deflections due to the myogenic oscillation. The oscillations of the two nephrons are not synchronized, as shown by the shift in time between the peaks in the two oscillations, which reflects the fact that the phase angle difference between the nephrons changes with time.

Figure 2*B* shows the renal plasma flow rate as a function of time in the same two nephron models, but this time coupled by vascular electrical conductances. The two oscillations in each nephron of the pair now are synchronized with each other: TGF with TGF and myogenic with myogenic. The TGF/myogenic ratio remains 5:1 in both nephrons. The phase angles between both pairs of oscillations are 0 and do not vary with time. The frequencies in both the TGF and the myogenic oscillations of each nephron changed from their values in the uncoupled state. These results satisfy the criteria for synchronization (27). The amplitudes of the TGF oscillation (defined as the square root of the TGF spectral power; see Table 5) in the two nephrons also changed with synchronization, increasing in the shorter nephron and decreasing in the longer. The amplitudes of the TGF oscillations in the two nephrons tended to converge with synchronization but did not become equal.

Tables 4 and 5 present the results of simulations among nephrons with descending limbs ranging in length from 2.75 to 4 mm, at 0.25-mm increments. In all cases, the coupling led to synchronization of both the TGF and the myogenic oscillations. In all cases, the myogenic:TGF coupling remained at 5:1.

Table 3. *Simulation results: effect of nephron length on period length and spectral power of the tubuloglomerular feedback oscillation in nephron plasma flow in single nephrons*

DLH Length, mm	Period Length, s	Spectral Power, nl/min^2
2.75	41.2	109.4
3.0	42.8	113.7
3.25	43.3	242.6
3.5	43.7	264.7
3.75	44.6	304.2
4.0	45.1	326.0

Nephron length is specified as the length of the descending limb of Henle's loop (DLH).

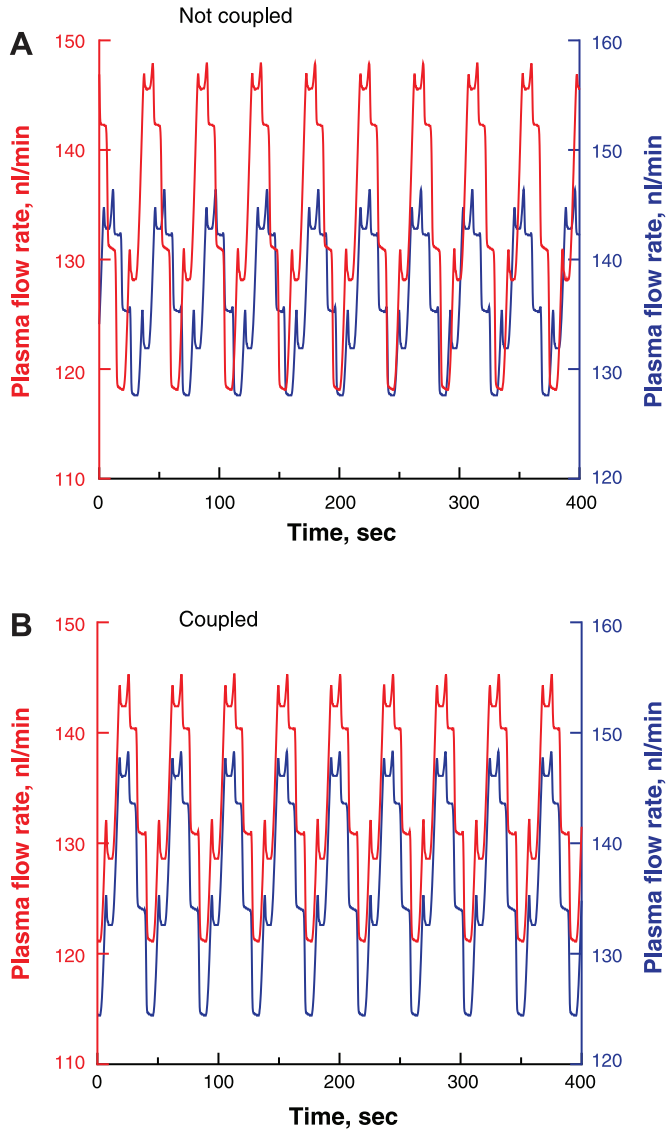

Fig. 2. Plasma flow rate in 2 nephrons as a function of time. The length of the descending limb is 3.0 mm in the blue tracing and 4.0 mm in the red. Note that the axes are offset against each other to permit easier visualization. *A*: nephrons are not coupled. *B*: nephrons are coupled by vascular electrical signal conduction.

In all cases, the amplitudes of the TGF oscillations, shown as spectral power within the frequency range 0.01–0.05 Hz, changed as a result of the coupling. We could not, however, deduce a rule governing the redistribution of spectral power between nephrons as a result of coupling.

Synchronization and stability of myogenic:TGF coupling. We next asked whether synchronization changes the stability of the model performance. We defined stability as the range of values of some parameter over which no change occurs in the solution of the model equations. We further defined no change to mean that the TGF activity remains a limit cycle in each nephron and synchronization of the TGF with the myogenic oscillation remains at 5:1. A particular case in point is the range of values of the parameter φ_n, which appears in *Eq. A20*. Adjustments in the value of this parameter permit changes in the frequency of the myogenic oscillation so that the ratio of

Table 4. *Simulation results: effect of nephron length on period length in coupled nephron pairs*

Nephron 2 DLH Length, mm	*Nephron 1* DLH Length, mm					
	2.75	3.0	3.25	3.5	3.75	4.0
4.0	42.6	43.7	44.1	44.4	44.9	45.2
3.75	42.5	43.6	43.9	44.2	44.7	
3.5	42.2	43.3	43.5	43.8		
3.25	42.1	43.1	43.4			
3.0	41.9	42.9				
2.75	41.4					

The axes are the length of the descending limb (mm); the elements in the table are period length (s).

the TGF:myogenic frequencies can be set to 5:1. In this set of simulations, we paired nephrons of identical lengths; in one nephron, φ_n was increased to find the maximum value while in the other φ_n was decreased to find the minimum. Each simulation was therefore conducted to find the maximum range of φ_n that would produce limit cycle TGF oscillations in both nephrons and a 5:1 ratio of the myogenic:TGF oscillations in each.

Figure 3 shows the range of values for φ_n that enable the system solutions to remain stable. The range is shown for single and paired nephrons as a function of the length of the descending limb of Henle's loop. The values of φ_n are presented as $2(\varphi_{n,max} - \varphi_{n,min})/(\varphi_{n,max} + \varphi_{n,min})$, where $\varphi_{n,max}$ and $\varphi_{n,min}$ are the maxima and minima, respectively, of the values of φ_n that confer stability, defined as persistence of limit cycle oscillations in both nephrons of the pair, and 5:1 myogenic:TGF oscillations in each. This form shows the parameter range divided by the average of those parameter values, for each length. The normalization is useful for comparison purposes because the value of $(\varphi_{n,max} + \varphi_{n,min})/2$ varies as a function of tubule length.

The figure shows that the stable range in both sets of simulations varies with the length of the descending limb. At all lengths, the stable range is greater in the simulations of coupled nephrons than with the single-nephron simulations. The effect is greatest in the shortest nephron (by a factor of 13.4) and least in the longest nephron (factor of 2.0). The results indicate that coupling two nephrons increases the stability of the system.

Table 5. *Simulation results: effect of nephron length on spectral power of the transforming growth factor oscillation in plasma flow rate in coupled nephron pairs*

Nephron 2 DLH Length, mm	*Nephron 1* DLH Length, mm					
	2.75	3.0	3.25	3.5	3.75	4.0
4.0	207.7	197.0	244.1	256.8	284.8	302.3
3.75	193.5	188.2	236.3	252.4	280.0	297.0
3.5	171.2	176.2	226.5	243.8	275.0	291.0
3.25	158.1	170.4	222.4	239.3	270.6	289.3
3.0	132.2	102.5	143.2	159.6	186.5	201.8
2.75	97.5	94.3	178.6	196.4	223.9	240.5

The axes are length of the descending limb (mm); the elements in the table are spectral power (nl/min^2).

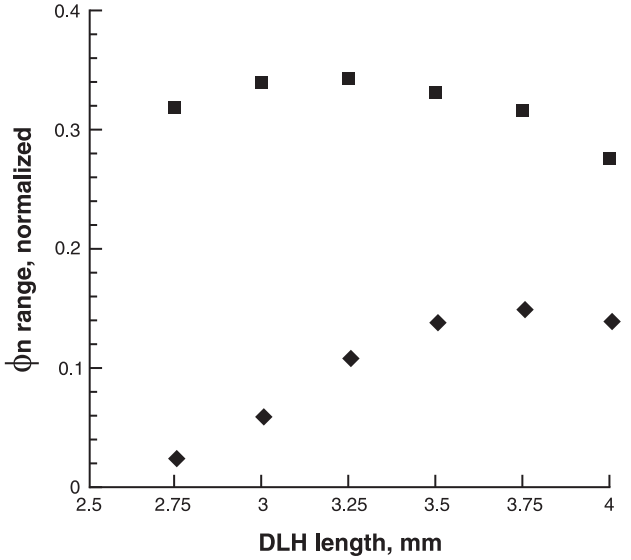

Fig. 3. Normalized range of φ_n, the parameter used to adjust the frequency of the myogenic oscillation, in single-nephron simulations (◆) and coupled 2-nephron simulations (■) as a function of the length of the descending limb of Henle's loop.

DISCUSSION

The purpose of this study was to determine the mechanism of synchronization of TGF and myogenic oscillations in nephrons whose blood flows are supplied from a common cortical radial artery. Experimental results showing synchronization were from nephrons whose arterioles satisfied this anatomic condition (33), and we sought to simulate those results.

The first hypothesis we tested was that TGF activation initiates membrane depolarization of arteriolar smooth muscle cells and that the depolarization spreads from the juxtaglomerular apparatus downstream along the afferent arteriole into the cortical radial artery, and finally upstream to other afferent arterioles originating from the same cortical radial artery. Dissected mouse juxtaglomerular apparatuses were exposed to ANNINE-6, a voltage-sensitive fluorescent dye that partitions into cell membranes. Administering the dye from the bathing solution permitted it to reach its highest concentrations in vascular smooth muscle cells. The activation of TGF by perfusion of the thick ascending limb adherent to the juxtaglomerular apparatus led to prompt depolarization in the afferent arteriole of the activated nephron, and that depolarization occurred promptly in the other afferent arterioles of the preparation. The depolarization in these other afferent arterioles was less than in the arteriole of the activated nephron.

The TGF-initiated depolarization has not been shown previously. TGF activation stimulates contraction of arteriolar smooth muscle, but it could do so by inducing membrane depolarization or by releasing Ca^{2+} from intracellular stores (18). Our result supports the role of membrane depolarization in causing the Ca^{2+} entry that triggers smooth muscle contraction, a conclusion supported by a number of experimental studies (2, 7, 14, 19). Another issue is the character of the propagation. Studies of propagated depolarization in nonrenal microcirculations have shown an electrotonic decline in membrane potential with distance, but none of these has analyzed arterioles with periodic vasomotion (8, 10, 36). The presence

of a self-sustained oscillation requires that we examine the possibility of regenerative propagation of action potentials. A regenerative process would maintain the level of depolarization throughout the length of the blood vessel. Our results are compatible with simple electrotonic current conduction. The conclusion is important for the simulation of synchronization. If the depolarization does not decline with distance, and if it is relatively slow, it would be necessary to simulate the membrane currents in each cell, a process that would increase the complexity of the arteriolar model. The fact that the depolarization in the renal afferent arteriole declines with distance and is relatively fast justifies the use of a simple ohmic network to account for the propagation events among the arterioles.

We then used two separate nephron models (21), each coupled by a conductance to a common electrical node. The node also had a connection to ground. The combined model was solved numerically. The model that simulates the TGF oscillation is based on the assumption that the negative feedback structure is the only source of the oscillation (11, 12). Recently, sustained oscillations in intracellular Ca^{2+} have been reported in podocytes and in cells of the cortical thick ascending limb epithelium (16, 26). The Ca^{2+} oscillations have frequencies similar to those found for tubular pressure and flow, but their functional significance remains to be established and are not included in the present model. We first used the combined model to estimate the conductance coupling the nephrons, by comparing the simulation results to experimental results (35). Arterioles of juxtamedullary nephrons had been exposed to depolarizing K^+ solutions applied in a thin, flowing stream to perfused afferent arterioles. The induced vasoconstriction was measured as a function of distance from the point of application of the high-K^+ solution, and the data were fitted to a single exponential. In the simulations, a 2-s pulse of current was applied to one afferent arteriole at a point close to the glomerulus. The simulated diameter change at the point of stimulation was measured, and also at the same point in the companion nephron. We varied the coupling conductance and the conductance to ground to find a best fit to the exponential defined by the experimental results.

The model structure can provide a single value of the ratio between the coupling conductance, g_{IN}, and conductance to ground, g_0, but not a unique value of either one. We had previously selected a value of the conductance coupling the two segments of the afferent arteriole, g_{IC}, by using the minimum value of the parameter that would permit synchronization of the two segments (21). In this study, we assumed that g_{IN} would be of the same approximate magnitude and adjusted g_0 accordingly. These values were then used to test for synchronization.

We paired nephrons of different lengths to test for synchronization. The length of the tubule determines the time required for a fluid wave to travel from the glomerulus to the macula densa, and the period of the oscillation therefore varies directly with the length. The results show synchronization for all nephron pairs. In each case, the frequencies in the two nephrons assumed a value intermediate between the frequencies in single nephrons. The myogenic oscillation remained coupled to the TGF oscillation in each nephron at a 5:1 ratio. Because there was a frequency adjustment to coupling in the TGF oscillation as a result of coupling, there must have been similar adjustments in the myogenic oscillation. The simulation results suggest that the estimated internephron conductance is sufficient to account for nephron synchronization. Pitman et al. (28) have simulated two coupled nephrons with variable time delays and found that the limit cycle oscillation persisted in both nephrons; theirs is a simpler nephron, with no myogenic mechanism.

In our earlier study (21), we used φ_n to control the oscillation frequency of the myogenic mechanism. In the afferent arteriolar model, the only membrane processes that participate in the myogenic oscillation are the K^+ and Ca^{2+} currents. The Ca^{2+} current can also be used to vary the timing of the myogenic oscillation, but because Ca^{2+} also determines myosin light chain phosphorylation, the response to a change in its conductance is complex. The response to variation of φ_n is limited to its effect on the oscillation frequency, an advantage in this context, and the reason for its selection. In the current study, using the single-nephron model with shorter nephrons, φ_n can be varied only over a range of a few percentage points of the average of the minimum and maximum values to provide 5:1 coupling. The range increases in the longer nephrons, probably because the amplitude of the TGF oscillation increases with nephron length, which should provide a stronger effect of TGF on the myogenic oscillation. For the simulations, this narrow range creates no difficulty, but in vivo one could imagine that the TGF and myogenic oscillations could often become unsynchronized; experimental results show that the desynchronization is uncommon in normal rats (33). We therefore examined the effect of variation of φ_n in coupled nephron pairs. The effect of coupling two nephrons was to extend the range of values of φ_n that would sustain self-sustained TGF oscillations coupled 5:1 to the myogenic oscillations in the same nephrons. As can be seen in Fig. 3, the effect of coupling was to extend the range of φ_n values by as much as 13-fold in the shortest nephrons and 2-fold in the longest. If we define stability as the persistence of a self-sustained TGF oscillation coupled 5:1 to the myogenic oscillation, coupling increases the stability of the system with respect to the value of φ_n. Loss of stability in this system leads primarily to a bifurcation to quasiperiodicity, period doubling, or deterministic chaos in TGF dynamics. Both the TGF and the myogenic oscillations remain synchronized in the two nephrons, but the destabilization is revealed as a loss of the self-sustained oscillation of TGF. Quasiperiodicity is less stable than a self-sustained oscillation and can lead to the development of chaos, and period doubling is a precursor to chaos (25).

In the two-nephron simulations using different values of φ_n, all other parameters of the system were left unchanged. Variation of φ_n in the model is one parameter that determines the frequency of the myogenic oscillation. The interaction with the TGF oscillation then establishes 5:1 synchronization. The stability limits indicate that the interactions between the two oscillations can only succeed in establishing synchronization over some range of the interactions, and not under all circumstances.

Limits of this sort are well known in theoretical studies of nonlinear oscillators (27), but it is worthwhile to explore their physiological implications in the kidney. Elsewhere, we suggested that because both the TGF and the myogenic oscillations are self-sustained, the systems generating them must be nonlinear (21). The interaction between nonlinear oscillators can give rise to several effects, including frequency and am-

plitude modulation of one oscillation by the other, synchronization of the oscillators, and bifurcations to chaos. We have shown frequency and amplitude modulation of the myogenic oscillation by TGF in experimental results (23), and TGF-myogenic synchronization in individual nephrons, synchronization of the TGF oscillations in two nephrons, and synchronization of the myogenic oscillations in the same two nephrons (33). We have also suggested that amplitude modulation of the myogenic oscillation by TGF could provide coordination of the actions of these two systems in response to fluctuations of arterial blood pressure (23). Coordination would be useful in permitting autoregulation to achieve an effective unified response to these fluctuations.

The dynamics of renal autoregulation in hypertensive rats are different from those in normotensive animals: TGF fluctuations are irregular, and there are infrequent synchronization of the myogenic mechanism with TGF; infrequent synchronization of TGF fluctuations in the paired nephrons; and infrequent synchronization of myogenic fluctuations in the paired nephrons (5, 6, 29, 33). If our formulation of the physiological implications of modulation in normotensive animals is correct, it follows that nephron coupling stabilizes the modulation and helps to ensure the coordinated action of TGF and the myogenic mechanism. The lack of synchronization effects in hypertensive animals then leads to the implication that coordination is less effective in hypertension, because of altered interactions between TGF and the myogenic mechanism. In the simulations presented in this paper, the stability was reduced by varying the dynamics of K^+ channels in arteriolar smooth muscle cells. Whether K^+ channel dynamics are altered in afferent arterioles of hypertensive rats must be determined experimentally, but there are very likely other parameter variations that could produce similar results.

The available data showing synchronization were collected from nephron pairs on the surface of the rat kidney (33, 37). The cortical radial artery typically supplies 20 nephrons of different tubule lengths (3), and the possibility needs to be considered that the synchronization spreads to more than a single pair. Electrotonic vascular signaling can propagate to nearby pairs or triplets of nephrons. The propagation of the electronic signals will be reinforced by the recruitment of single small groups of nephrons, and this process should be able to propagate for some distance, possibly including all the nephrons derived from that cortical radial artery. In addition, the synchronization of the terminal nephron pair will induce an oscillation of blood flow in the cortical radial artery, which will reinforce the electrically induced synchronization.

In a previous study, we have simulated a 22-nephron cluster derived from one cortical radial artery. The simulated nephrons included a majority of cortical nephrons and smaller numbers of medullary nephrons (22). The model used to simulate each nephron (1) was much simpler than the one used in this study, had no myogenic mechanism, and modeled coupling phenomenologically, without specifying a mechanism. That study predicted extensive synchronization and an oscillation in blood flow in the cortical radial artery. The oscillations of cortical nephrons synchronized among themselves but not with medullary nephrons. The failed synchronization led to different dynamic patterns, including oscillations, quasiperiodicity, and chaos. That model predicted that the strength of the coupling between nephrons could determine whether these different patterns emerged. The results of the current study suggest that the coupling of TGF with the myogenic mechanism stabilizes the oscillations of each. Whether coupling has a similar effect when additional nephrons are included remains to be established.

Glossary

Subscripts

A	Afferent arteriole
E	Efferent arteriole
GC	Glomerular capillary
IN	Internepron
I	Interstitial
S	NaCl
T	Renal tubule

Independent Variables

t	Time, s
z	Tubule position, cm
z_{GC}	Glomerular capillary position, cm

Dependent Tubular Variables

$C_s(z,t)$	NaCl concentration, mM
$P(z,t)$	Pressure, mmHg
$Q(z,t)$	Flow, cm^3/s

Dependent Glomerular Capillary Variable

$C(z_{GC})$	Glomerular capillary protein concentration, g/l

Auxiliary Variables

$J(z,t)$	Solute (mmol/min) or volume (nl/min) flux
$R(t)$	Vascular resistance, $dyn \cdot s \cdot cm^{-5}$
$r(z,t)$	Tubular radius, cm

Dependent Arteriolar Variables

$Ca_i(Ca_i,m_\infty,v,t)$	Intracellular Ca concentration, mM
$n(v,Ca_i,t)$	Fraction of open K channels
$v(Ca_i,n,t)$	Membrane electrical potential difference, mV
$x(x,P_A,t)$	Length of parallel elastic element, cm
$y(y,\xi,\omega,t)$	Length of the contractile element, cm
$\omega(\omega,\xi,t)$	Fraction of actual: possible actin-myosin cross bridges

Auxiliary Arteriolar Variables

$m_\infty(v)$	Equilibrium distribution of Ca open-channel states
$n_\infty(v,Ca_i)$	Equilibrium distribution of K open-channel states
$u(x,y)$	Length of series elastic component, cm
$\xi(Ca_i)$	Fraction of phosphorylated myosin light chain

APPENDIX

TGF: Tubule Model

Tubule model. The equations describing pressure, P_T, and flow, Q_T, for a noncompressible Newtonian fluid in a compliant, reabsorbing tubule at low Reynolds number are

$$\frac{\partial P_T}{\partial z} = -\frac{\rho}{\pi r^2}\frac{\partial Q_T}{\partial t} - \frac{8\eta}{\pi r^4}Q_T, \quad 0 \le z \le Z, t \ge 0 \qquad (A1)$$

and

$$\frac{\partial Q_T}{\partial z} = -2\pi r\frac{\partial r}{\partial P_T}\frac{\partial P_T}{\partial t} - J_v(z), \quad 0 \le z \le Z, t \ge 0 \qquad (A2)$$

where ρ is the fluid density and η is the viscosity.

The boundary conditions for *Eqs. A1* and *A2* are the tubular inflow rate, $Q_T(0)$, as calculated from the equations of the glomerular model, and the tubular outlet pressure, which is estimated from experimental measurements

$$P_T(Z) = \frac{Q_T(Z)}{(\alpha_T P_T(Z) + \beta_T)^4} \qquad (A3)$$

The proximal tubule, the descending and the ascending limbs of the loop of Henle are each represented separately.

Proximal tubular fluid reabsorption, J_v is

$$J_v = \kappa \exp(-\theta z) \qquad (A4)$$

For the descending limb of Henle's loop, J_v is a function of the transtubular gradient of solute

$$J_v = L_p(C_s - C_I) \qquad (A5)$$

To reduce the number of constants, L_p is defined here to include the universal gas constant and the absolute temperature, and is defined as $mol^{-1}\cdot s^{-1}$.

In the ascending limb of the Henle's loop, volume reabsorption is 0.

Tubular radius is expressed as a linear function of transtubular pressure

$$r(z) = \gamma(P_T(z) - P_I) + r_0 \qquad (A6)$$

NaCl is treated as a single solute, s. For a solute s in a reabsorbing tubule with an axial flow, Q_T, mass balance requires that

$$\frac{\partial AC_s}{\partial t} = -\frac{\partial Q_T C_s}{\partial z} - J_s \qquad (A7)$$

where A is the tubule cross-sectional area, and C_S is the solute concentration.

The proximal tubule reabsorbs tubular fluid isosmotically. NaCl is the principal osmotically active component, C_S is assumed to be constant in that segment, and *Eq. A7* is solved only for the loop of Henle. For the initial condition, C_S is set equal to the interstitial concentration, 150 mM, at the beginning of the descending limb.

J_S is specified as a passive transport term in the descending limb of Henle's loop, and as a sum of a passive transport term and an active term following Michaelis-Menten kinetics in the ascending limb of Henle's loop.

Thus

$$J_s = L_s(C_s - C_I) + \frac{V_{max}C_s}{K_m + C_s} \qquad (A8)$$

where $V_{max} = 0$ for the descending limb, since there is no active transport in that segment.

The interstitial NaCl concentration, C_I, varies linearly from 150 mM at the corticomedullary boundary to 285 mM at the border between the inner and outer medulla, and by $C_I(z^* + z_{DLH_0}) = 285 + 20\tanh(.023(z^* - z^*_{DLH_0}))$ thereafter; $z^*_{DLH_0}$ is the length of the tubule from glomerulus to the bend of Henle's loop of cortical nephrons divided by the spatial step size, and z^* is the distance from the glomerulus in the additional length of descending limb, divided by the spatial step size. For the cortical thick ascending limb of the loop of Henle, C_I was set to 150 mM.

TGF: afferent arteriolar model. The action of tubuloglomerular feedback, is described by a logistic equation

$$\vartheta = \vartheta_{max} - \frac{\psi}{1 + \exp[k(C_s(md) - C_{1/2})]} \qquad (A9)$$

where V_{max} is the maximum obtainable response, Ψ is the dynamic range, $C_s(md)$ is the NaCl concentration at the macula densa, k is the feedback gain, and $C_{1/2}$ is the NaCl concentration that gives the half-maximum response.

Glomerular model. Glomerular capillaries are impermeable to protein and glomerular filtration rate, $Q_T(0)$, is therefore

$$Q_T(0) = \left(1 - \frac{C_A}{C_E}\right)Q_A \qquad (A10)$$

The plasma flow, Q_A, to the glomerular capillaries is

$$\frac{Q_A}{(1 - Ht_A)} = \frac{(P_A - P_{GC})}{R_A} \qquad (A11)$$

Glomerular capillary hydrostatic pressure, P_{GC}, is

$$P_{GC} = R_E\left[\frac{Q_A}{(1 - Ht_A)} - Q_T(0)\right] + \frac{Q_A R_v}{1 - Ht_A} \qquad (A12)$$

which is obtained by assuming that afferent blood flow less the glomerular filtrate rate, $Q_T(0)$, passes through the efferent arteriole and that thereafter the tubular reabsorbate is added to the efferent blood flow, which then passes through a distal resistance, R_v, to the venous compartment, in which the hydrostatic pressure is assumed to be zero.

The filtration process that causes the change in protein concentration is proportional to the sum of local hydrostatic and oncotic pressure differences

$$\frac{dC}{dz_{GC}} = \frac{K_f}{LQ_A C_A}C^2[P_{GC} - P_T(0) - \Pi(C)] \qquad (A13)$$

where z_{GC} is the fractional position along the glomerular capillary, K_f is the filtration coefficient, and L is the length of an idealized glomerular capillary. The initial condition, $P_{GC}(0)$, is derived from the arterial pressure and the calculation of afferent arteriolar vascular resistance, as detailed below.

The plasma oncotic pressure, $\Pi(C)$, is found from

$$\Pi(C) = a_{GC}C + b_{GC}C^2 \qquad (A14)$$

according to Deen et al. (9).

Myogenic Model

The preglomerular vascular bed is modeled as three segments in series. The first segment represents the larger renal vessels which do not contribute to autoregulation, and whose resistance R_{A1} is therefore assumed to be constant. The second and third segments, which are downstream from the first, each have a variable resistance under the control of both the myogenic mechanism and TGF. The resistance in these segments is given as

$$R_{A,j} = \frac{\Lambda_j}{r_j^4}, \; j = 2, 3 \qquad (A15)$$

where Λ_j combines the segment's length and the blood viscosity.

Each of the two arteriolar segments is modeled separately as a set of six ordinary differential equations and associated constituitive relationships.

Transport of ions and membrane potential. The equilibrium distribution of Ca open-channel states, m_∞, as a function of the membrane voltage, v_j, of the arteriolar segment j is

$$m_{\infty,j}(v_j) = 0.5\left(1 + \tanh\frac{v_j - v_1}{v_2}\right), j = 2, 3 \quad (A16)$$

where v_1 is the voltage at which half the channels are open, v_2 is a measure of the spread of the distribution, and j are the second and third arteriolar segments. This equation is intended to represent a mixture of L- and T-type Ca channels.

For K channels, the distribution is

$$n_{\infty,j}(v_j, \mathrm{Ca_i}) = 0.5\left(1 + \tanh\frac{v_j - v_{3,j}}{v_4}\right), j = 2, 3 \quad (A17)$$

where

$$v_{3,j} = -\frac{v_5}{2}\tanh\frac{\mathrm{Ca}_{i,vj} - \mathrm{Ca}_3}{\mathrm{Ca}_4} + v_6, j = 2, 3 \quad (A18)$$

Equation A18 provides a Ca-dependent shift in the distribution of K open states with respect to membrane voltage. The time course of the fraction of open K channels, n, is given by

$$\frac{dn_j}{dt} = \lambda(v_j)(n_{\infty,vj}(v_j, \mathrm{Ca}_{i,j}) - n_j), j = 2, 3 \quad (A19)$$

where

$$\lambda(v_j) = \phi_n \cosh\frac{v_j - v_{3,j}}{2v_4}, j = 2, 3 \quad (A20)$$

The rate of change of the membrane potential is related to membrane currents by

$$C_A\frac{dv^\circ_j}{dt} = \begin{cases} -I_{L,j} - I_{K,j} - I_{Ca,j} - I_{IC} - I_{IN}, & j = 2 \\ -I_{L,j} - I_{K,j} - I_{Ca,j} - I_{IC}, & j = 3 \end{cases} \quad (A21)$$

where C_A is membrane capacitance, and $I_{L,j}$, $I_{K,j}$, $I_{Ca,j}$ are the leak, potassium, and calcium currents of the jth arteriolar segment, respectively, I_{IC} is intercellular current, and I_{IN} is internephron current. Assuming an ohmic voltage-current relationship

$$C_A\frac{dv_j}{dt} = \begin{cases} -g_L(v_j - v_L) - g_K n_j(v_j - v_K) - g_{Ca,j,c}m_{\infty,j}(v_j - v_{Ca}) \\ -g_0(v_j - v_k) - g_{IN}(v_j - v_{node}), \quad j = 2, \quad k = 3 \\ -g_L(v_j - v_L) - g_K n_j(v_j - v_K) - g_{Ca,j,c}m_{\infty,j}(v_j - v_{Ca}) \\ \quad -g_0(v_k - v_j), j = 3, k = 2 \end{cases} \quad (A22)$$

Applying Kirchhoff's first law, $\Sigma I = 0$, to the node yields

$$v_{node} = \frac{g_{IN}(v_{21} + v_{22})}{(2g_{IN} - g_0)} \quad (A23)$$

where g_L, g_K, g_{Ca}, g_{IC}, and g_{IN} are the whole-cell membrane conductances for the leak, K, Ca, intercellular, and internephron currents, respectively, v_L, v_K, and v_{Ca} are the corresponding Nernst potentials, and $g_{Ca,j,c} = (1 + \zeta\vartheta_j)g_{Ca}$.$\vartheta_j$ is the input from TGF to the jth arteriolar segment, and ζ is the TGF myogenic coupling parameter. The coefficient $g_{Ca,j,c}$ therefore represents the membrane Ca conductance coupled to TGF in the jth segment. In the experiments reported in this study and previous ones (21, 23), $\zeta_2 = \zeta_3/3$ The TGF input, ϑ_j, varies approximately symmetrically about 0.The rate of change of total Ca concentration in the cytosol is given by

$$\frac{d\mathrm{Ca}_{T,j}}{dt} = -\alpha_A g_{Ca,j,c}m_\infty(v_j - v_{Ca}) - k_{Ca}\mathrm{Ca}_{i,j}, j = 2, 3 \quad (A24)$$

where $\alpha_A = 1/2\beta_A v_{cell}F$,$\beta_A$ is the fraction of the total cell volume occupied by the cytosol, V_{cell} is the total cell volume, F is Faraday's constant, and k_{Ca} is the first-order rate constant for Ca removal from the cytosol. By assuming that cytosolic free Ca is in equilibrium with various Ca buffers whose total concentration is B_T and that can be represented by a single equilibrium constant, K_d, one may arrive at

$$\frac{d\mathrm{Ca}_{i,j}}{dt} = -(\alpha_A g_{Ca,j,c}m_\infty(v_j - v_{Ca}) - k_{Ca}\mathrm{Ca}_{i,j})\varpi, \quad j = 2, 3 \quad (A25)$$

where

$$\varpi_j = \frac{(K_d + \mathrm{Ca}_{i,j})^2}{(K_d + \mathrm{Ca}_{i,j})^2 + K_d B_T}. \quad (A26)$$

Myosin light chain phosphorylation. Activation of smooth muscle is assumed to occur in response to Ca-dependent phosphorylation of myosin light chain. One assumes that the kinetics of phosphorylation are rapid compared with the time scale of the vascular events, and defines ξ as the fraction of myosin light chain sites that are phosphorylated.

$$\xi_j = \frac{\mathrm{Ca}^q_{i,j}}{\mathrm{Ca}^q_{im} + \mathrm{Ca}^q_{i,j}}, j = 2, 3 \quad (A27)$$

We describe the relationship between phosphorylated light chain myosin and cross bridge formation phenomenologically in terms of a binding distribution. Letting ω_j represent the fraction formed of the total possible cross bridges in the jth arteriolar segment, we arrive at the expression

$$\frac{d\omega_j}{dt} = k_\xi\left(\frac{\xi_j}{\xi_m + \xi_j} - \omega_j\right), j = 2, 3 \quad (A28)$$

Wall stress and contraction velocity. The contractile mechanism has length y, the series elastic component length u, and the parallel elastic component length $x = u + y$. The stresses σ normal to the surface of a longitudinal slice, S_A, through the vessel wall and associated with each element are

$$\sigma_x = x_3\left(1 + \tanh\frac{x^* - x_1}{x_2}\right) + x_4(x^* - x_5) - x_8\left(\frac{x_6}{x^* - x_7}\right)^2 - x_9 \quad (A29)$$

$$\sigma_u = u_2\exp(u_1 u/x_0) - u_3 \quad (A30)$$

and

$$\sigma_y = \frac{\omega}{\omega_{ref}}\quad\frac{\exp\left(-\frac{(y/x_0 - y_0)^2}{2s(y/x_0)^2}\right) - y_3}{1 - y_3} \quad (A31)$$

where $x^* = x/x_0$, x_0 is a reference length, $u = (x - y)$, $s(y) = [y_1/(y + y_2)]^{y_4}$ and $\omega_{ref} = \omega(\mathrm{Ca}_{i,ref})/(\xi_m + \xi(\mathrm{Ca}_{i,ref}))$ The x_{1-9},u_{1-3}, and y_{1-3} are coefficients used to fit the various expressions to data from the literature.

The force-velocity relationship for the contractile mechanism is given by

$$\frac{dy}{dt} = -x_0 v_{ref}\frac{\xi}{\xi_{ref}}a_A\frac{1 - \frac{\sigma_u}{\sigma_y}}{a_A + \frac{\sigma_u}{\sigma_y}}, \quad 0 \le \frac{\sigma_u}{\sigma_y} \le 1,$$

or

$$\frac{dy}{dt} = x_0 c_A\left(\exp\left(b_A\left(\frac{\sigma_u}{\sigma_y} - d_A\right)\right) - \exp(b_A(1 - d_A))\right), \quad 1 \le \frac{\sigma_u}{\sigma_y} \quad (A32)$$

where v_{ref}, a_A, b_A, c_A, and d_A are constants.

The hoop forces f acting on a longitudinal section S_A of the blood vessel wall are given by

$$f_{\Delta P} = \frac{1}{2}\Delta P\left(\frac{x}{\pi} - \frac{A}{x}\right), \quad x > \sqrt{\pi A} \tag{A33}$$

where ΔP is the transmural pressure difference between the vascular wall and the interstitial space, and A is the cross-sectional area of the vascular smooth muscle cells.

$$f_x = w_e S_A \sigma_x \sigma_0 \tag{A34}$$

$$f_u = w_m S_A \sigma_u \sigma_0 \tag{A35}$$

w_e and w_m are weighting factors, and σ_0 is a reference stress.

The rate of change of the circumference x is given by

$$\frac{dy}{dt} = \frac{1}{\tau}(f_{\Delta P} - f_x - f_u) \tag{A36}$$

subject to the geometric compatibility condition

$$x = u + y \tag{A37}$$

GRANTS

This work was supported in part by National Institutes of Health Grant R01-EB-003508 to D. J. Marsh, the European Union through the Network of Excellence BioSim (contract no. LSHB-CT-2004–005137), a travel grant from the Lundbeck Foundation of Copenhagen, Denmark (to N.-H. Holstein-Rathlou and D. J. Marsh), and the Danish Research Council for Health and Disease (to N.-H. Holstein-Rathlou).

REFERENCES

1. **Barfred M, Mosekilde E, Holstein-Rathlou NH.** Bifurcation analysis of nephron pressure and flow regulation. *Chaos* 6: 280–287, 1996.
2. **Carmines PK, Navar LG.** Disparate effects of Ca channel blockade on afferent and efferent arteriolar responses to ANG II. *Am J Physiol Renal Fluid Electrolyte Physiol* 256: F1015–F1020, 1989.
3. **Casellas D, Dupont M, Bouriquet N, Moore LC, Artuso A, Mimran A.** Anatomic pairing of afferent arterioles and renin cell distribution in rat kidneys. *Am J Physiol Renal Fluid Electrolyte Physiol* 267: F931–F936, 1994.
4. **Chen YM, Yip KP, Marsh DJ, Holstein-Rathlou NH.** Magnitude of TGF-initiated nephron-nephron interactions is increased in SHR. *Am J Physiol Renal Fluid Electrolyte Physiol* 269: F198–F204, 1995.
5. **Chon KH, Chen YM, Marmarelis VZ, Marsh DJ, Holstein-Rathlou NH.** Detection of interactions between myogenic and TGF mechanisms using nonlinear analysis. *Am J Physiol Renal Fluid Electrolyte Physiol* 267: F160–F173, 1994.
6. **Chon KH, Raghavan R, Chen YM, Marsh DJ, Yip KP.** Interactions of TGF-dependent and myogenic oscillations in tubular pressure. *Am J Physiol Renal Physiol* 288: F298–F307, 2005.
7. **Conger JD, Falk SA.** KCl and angiotensin responses in isolated rat renal arterioles: effects of diltiazem and low-calcium medium. *Am J Physiol Renal Fluid Electrolyte Physiol* 264: F134–F140, 1993.
8. **Crane GJ, Kotecha N, Luft SE, Neild TO.** Electrical coupling between smooth muscle and endothelium in arterioles of the guinea pig small intestine. *Phys Med Biol* 46: 2421–2434, 2001.
9. **Deen WM, Robinson CR, Brenner BM.** A model of glomerular ultrafiltration in the rat. *Am J Physiol* 223: 1183, 1972.
10. **Diep HK, Vigmond EJ, Segal SS, Welsh DG.** Defining electrical communication in skeletal muscle resistance arteries; a computational approach. *J Physiol* 568.1: 267–281, 2005.
11. **Holstein-Rathlou NH, Marsh DJ.** Oscillations of tubular pressure, flow, and distal chloride concentration in rats. *Am J Physiol Renal Fluid Electrolyte Physiol* 256: F1007–F1014, 1989.
12. **Holstein-Rathlou NH, Marsh DJ.** A dynamic model of the tubuloglomerular feedback mechanism. *Am J Physiol Renal Fluid Electrolyte Physiol* 258: F1448–F1459, 1990.
13. **Holstein-Rathlou NH, Marsh DJ.** Renal blood flow regulation and arterial pressure fluctuations: a case study in nonlinear dynamics. *Physiol Rev* 74: 637–681, 1994.
14. **Iversen BM, Arendshorst WJ.** ANG II and vasopressin stimulate calcium entry in dispersed smooth muscle cells of preglomerular arterioles. *Am J Physiol Renal Physiol* 274: F498–F508, 1998.
15. **Kallskog O, Marsh DJ.** TGF-initiated vascular interactions between adjacent nephrons in the rat kidney. *Am J Physiol Renal Fluid Electrolyte Physiol* 259: F60–F64, 1990.
16. **Komlosi P, Banizs B, Fintha A, Steele S, Zhang ZR, Bell PD.** Oscillating cortical thick ascending limb cells at the juxtaglomerular apparatus. *J Am Soc Nephrol* 19: 1940–1946, 2008.
17. **Kuhn B, Fromherz P, Denk W.** High sensitivity of Stark-shift voltage-sensing dyes by one- or two-photon excitation near the red spectral edge. *Biophys J* 87: 631–639, 2004.
18. **Loutzenhiser K, Loutzenhiser R.** Angiotensin II-induced Ca^{2+} influx in renal afferent and efferent arterioles: differing roles of voltage-gated and store-operated Ca^{2+} entry. *Circ Res* 87: 663–670, 2000.
19. **Loutzenhiser R, Hayashi K, Epstein M.** Divergent effects of KCl-induced depolarization on afferent and efferent arterioles. *Am J Physiol Renal Fluid Electrolyte Physiol* 257: F561–F564, 1989.
20. **Marsh DJ, Martin CM.** Effects of diuretic states on collecting duct fluid flow resistance in the hamster kidney. *Am J Physiol* 229: 13–17, 1975.
21. **Marsh DJ, Sosnovtseva OV, Chon KH, Holstein-Rathlou NH.** Nonlinear interactions in renal blood flow regulation. *Am J Physiol Regul Integr Comp Physiol* 288: R1143–R1159, 2005.
22. **Marsh DJ, Sosnovtseva OV, Mosekilde E, Holstein-Rathlou N-H.** Vascular coupling induces synchronization, quasiperiodicity, and chaos in a nephron tree. *Chaos* 17: 015114, 2007.
23. **Marsh DJ, Sosnovtseva OV, Pavlov AN, Yip KP, Holstein-Rathlou NH.** Frequency encoding in renal blood flow regulation. *Am J Physiol Regul Integr Comp Physiol* 288: R1160–R1167, 2005.
24. **Nordsletten DA, Blackett S, Bentley MD, Ritman EL, Smith NP.** Structural morphology of renal vasculature. *Am J Physiol Heart Circ Physiol* 291: H296–H309, 2006.
25. **Ott E.** *Chaos in Dynamical Systems*. Cambridge, UK: Cambridge Univ. Press, 2002.
26. **Peti-Peterdi J.** Calcium wave of tubuloglomerular feedback. *Am J Physiol Renal Physiol* 291: F473–F480, 2006.
27. **Pikovsky A, Rosenblum M, Kuerths J.** *Synchronization*. Cambridge, UK: Cambridge Univ. Press, 2001.
28. **Pitman EB, Zaritski RM, Kesseler KJ, Moore LC, Layton HE.** Feedback-mediated dynamics in two coupled nephrons. *Bull Math Biol* 66: 1463–1492, 2004.
29. **Raghavan R, Chen X, Yip KP, Marsh DJ, Chon KH.** Interactions between TGF-dependent and myogenic oscillations in tubular pressure and whole kidney blood flow in both SDR and SHR. *Am J Physiol Renal Physiol* 290: F720–F732, 2006.
30. **Sejnowski TJ, Paulsen O.** Network oscillations: emerging computational principles. *J Neurosci* 26: 1673–1676, 2006.
31. **Singer W.** Time as coding space? *Curr Opin Neurobiol* 9: 189–194, 1999.
32. **Singer W.** Consciousness and the binding problem. *Ann NY Acad Sci* 929: 123–146, 2001.
33. **Sosnovtseva OV, Pavlov AN, Mosekilde E, Yip KP, Holstein-Rathlou NH, Marsh DJ.** Synchronization among mechanisms of renal autoregulation is reduced in hypertensive rats. *Am J Physiol Renal Physiol* 293: F1545–F1555, 2007.
34. **Von Rosenburg DU.** *Methods for the Numerical Solution of Partial Differential Equations.* New York, NY: Elsevier, 1969.
35. **Wagner AJ, Holstein-Rathlou NH, Marsh DJ.** Internephron coupling by conducted vasomotor responses in normotensive and spontaneously hypertensive rats. *Am J Physiol Renal Physiol* 272: F372–F379, 1997.
36. **Yamamoto Y, Klemm MF, Edwards FW, Suzuki H.** Intracellular electrical communication among smooth muscle and endothelial cells in guinea-pig mesenteric arterioles. *J Physiol* 535.1: 181–185, 2001.
37. **Yip KP, Holstein-Rathlou NH, Marsh DJ.** Dynamics of TGF-initiated nephron-nephron interactions in normotensive rats and SHR. *Am J Physiol Renal Fluid Electrolyte Physiol* 262: F980–F988, 1992.